Joint Beamforming Design for Dual-Functional MIMO Radar and Communication Systems Guaranteeing Physical Layer Security

Fuwang Dong, *Member, IEEE*, Wei Wang, *Senior Member, IEEE*, Xin Li, Fan Liu, *Member, IEEE*, Sheng Chen, *Fellow, IEEE*, and Lajos Hanzo, *Life Fellow, IEEE*

***Abstract*—The dual-functional radar and communication (DFRC) technique constitutes a promising next-generation wireless solution, due to its benefits in terms of power consumption, physical hardware, and spectrum exploitation. In this paper, we propose sophisticated beamforming designs for multi-user DFRC systems by additionally taking the physical layer security (PLS) into account. We show that appropriately designed radar waveforms can also act as the traditional artificial noise conceived for drowning out the eavesdropping channel and for attaining increased design degrees of freedom (DoF). The joint beamforming design is formulated as a non-convex optimization problem for striking a compelling trade-off amongst the conflicting design objectives of radar transmit beampattern, communication quality of service (QoS), and the PLS level. Then, we propose a semidefinite relaxation (SDR)-based algorithm and a reduced-complexity version to tackle the non-convexity, where the globally optimal solutions are found. Moreover, a robust beamforming method is also developed for considering realistic imperfect channel state information (CSI) knowledge. Finally, simulation results are provided for corroborating our theoretical results and show the proposed methods' superiority.**

***Index Terms*—Dual-functional radar and communication system, joint beamforming design, physical layer security, multi-user MIMO.**

Manuscript received 29 June 2022; revised 3 October 2022; accepted 28 December 2022. Date of publication 3 January 2023; date of current version 15 February 2023. This work was supported in part by the National Natural Science Foundation under Grant 62271163, and in part by the Fundamental Research Funds for the Central Universities under Grant 3072022QBZ0401 and Grant 3072021CFT0404. The work of Fan Liu was supported in part by the National Natural Science Foundation of China under Grant 62101234, and in part by the Young Elite Scientist Sponsorship Program by the China Association for Science and Technology (CAST) under Grant YESS20210055. The work of Lajos Hanzo was supported in part by the Engineering and Physical Sciences Research Council under Project EP/W016605/1 and Project EP/P003990/1 (COALESCE), and in part by the European Research Council's Advanced Fellow Grant QuantCom under Grant 789028. *(Corresponding author: Wei Wang.)*

Fuwang Dong is with the Department of Electronic and Electrical Engineering, Southern University of Science and Technology, Shenzhen 518055, China (e-mail: dongfw@sustech.edu.cn).

Wei Wang and Xin Li are with the College of Intelligent System Science and Engineering, Harbin Engineering University, Harbin 150001, China (e-mail: wangwei407@hrbeu.edu.cn; xinxin_forever@126.com).

Fan Liu is with the Department of Electronic and Electrical Engineering, Southern University of Science and Technology, Shenzhen 518055, China, and also with Peng Cheng Laboratory, Shenzhen 518066, China (e-mail: liuf6@sustech.edu.cn).

Sheng Chen and Lajos Hanzo are with the School of Electronic and Computer Science, University of Southampton, SO17 1BJ Southampton, U.K. (e-mail: sqc@ecs.soton.ac.uk; lh@ecs.soton.ac.uk).

Digital Object Identifier 10.1109/TGCN.2022.3233863

I. Introduction

THE PROLIFERATION of wireless mobile services exhibits an exponential trend, leading to a scarcity of spectral resources and to escalating spectrum prices. For example, it has been reported that the number of connected devices is expected to be 80 billion by 2030 with an annual growth rate of around 25%, and that of the active Internet of Things (IoT) devices will reach 24.1 billion by 2030 [1], [2]. Recently, the concept and scope of *Integrated Sensing and Communication (ISAC)* technology have been formally defined in [3], [4], enabling sensing and communication simultaneously in the same frequency band or/and hardware platform, which can significantly improve the resource utilization. Due to the numerous advantages offered by ISAC, it is envisioned to be a promising technique in terms of supporting autonomous vehicles [5], [6] and the IoT in 6G wireless networks [7].

There are two main ISAC categories in terms of transmitted signal: radar and communication spectrum coexistence and dual functional radar-communication (DFRC) [8], [9]. In this paper, we consider a DFRC system, which transmits dual-functional signals/waveforms from a single hardware platform, to gain benefits from joint sensing and signaling operations via real-time cooperation. The main motivation of transmit beamforming is to synthesize multiple beams towards both the communication users and the radar targets by exploiting the associated spatial degrees of freedom (DoF). In [10], the authors considered the radar targets as virtual downlink users encountering a line of sight (LoS) channel. Therefore, the beamforming matrix was designed for closely matching the desired radar beampattern, while simultaneously guaranteeing the signal to interference and noise ratio (SINR) attained by the downlink users. Furthermore, the authors of [11], [12] studied the associated symbol/waveform level probing signal design issues, where the multi-user interference energy was minimized under the similarity and constant modulus constraints of the radar waveform. However, the above-mentioned schemes only utilize the communication waveform as the DFRC waveform to implement target detection, hence leading to a DoF reduction, thereby to a radar performance degradation. To this end, the authors of [13] firstly proposed a jointly precoded individual communication and radar waveforms based scheme, where the communication signal can be regarded as a special case relying on nullifying the dedicated radar waveforms.

2473-2400 © 2023 IEEE. Personal use is permitted, but republication/redistribution requires IEEE permission.
See https://www.ieee.org/publications/rights/index.html for more information.

Authorized licensed use limited to: UNIVERSITY OF SOUTHAMPTON. Downloaded on February 16,2023 at 09:13:26 UTC from IEEE Xplore. Restrictions apply.

TABLE I
OUR CONTRIBUTIONS IN CONTRAST TO THE STATE-OF-THE-ART

	[10]	[13]	[17]	[18]	[19]	Our work
Secure Transmission			✓	✓	✓	✓
Jointly precoded communication and radar waveforms		✓				✓
Precoder design rather than covariance matrix	✓	✓	✓			✓
Radar beampattern optimization	✓	✓				✓
Multiple users	✓	✓			✓	✓
Imperfect CSI estimations					✓	✓
Multiple eavesdroppers						✓
Using radar signal as artificial noise						✓
Tight solution for PLS design						✓

Therefore, by exploiting the inherent advantages of the radar waveform, the DoF erosion can be efficiently compensated, hence resulting in target detection performance improvements, especially for a small number of downlink users.

Another critical problem in the DFRC system, which has been largely overlooked in the relevant literature, is how to guarantee the privacy and security of the desired information [14]. The DFRC base station (BS) transmits the dual-functional probing waveform for detection purposes, but also sends confidential information to the targets. Evidently, private information might be leaked to the targets, which may act as potential eavesdroppers (Eves). Recently, several schemes have been proposed for guaranteeing secure data transmission by exploiting constructive interference [15], frequency hopping [16], and additional artificial noise (AN) [17], [18], [19], etc. As a low complexity yet powerful technique, the AN method has been widely harnessed in the communication community for enhancing the physical layer security (PLS). The basic principle of AN-aided secure transmission is that of contaminating the transmit signal by well-designed AN to degrade Eve's reception without affecting the legitimate users (LUs) [20].

In [17], several optimization problems, including secrecy rate maximization, target return SINR maximization, and transmit power minimization were formulated for a DFRC system in the presence of a single target and a single communication receiver. To tackle the non-convexity of the secrecy rate expression, an approximate algorithm based on the first-order Taylor expansion was proposed, which however resulted in a performance gap between the original non-convex problem and the approximated one. The authors of [18] considered a unified joint passive radar and communication system, where the SNR at the passive radar receiver was maximized, while keeping the secrecy rate above a certain target. Moreover, several practical constraints, such as realistic target direction estimation and imperfect channel state information (CSI) were taken into account in the associated robust beamforming proposal of [19]. However, at the time of writing, most of the contributions on secure DFRC systems have the following two drawbacks: (1) They only design the covariance matrix of the AN, yet no further analysis of the DFRC system's radar detection is offered; (2) Several relaxation algorithms are used such as Taylor expansions or semidefinite relaxation (SDR) techniques, but the performance loss compared to the original non-convex problem is overlooked.

Motivated by filling the above-mentioned knowledge gap in the literature, we develop jointly precoded communication and radar waveforms for secure transmission in a multiple-input multiple-output (MIMO) DFRC system inspired by [13], serving multiple LUs and detecting the targets simultaneously. On one hand, the DFRC platform relying on the ISAC technique eliminates duplication in the system's hardware. On the other hand, the bespoke transmit signals can simultaneously meet the requirements of radar, communications, and PLS, circumventing redundancy in the resource consumption for each functionality, hence also the power dissipation. Compared to the current DFRC schemes such as those in [10], [11], [12], [19], our method achieves superior radar detection performance thanks to the increased DoFs attained by the additional radar waveforms. In contrast to [13], the PLS level is also considered in our work, where the targets may act as potential Eves. The radar waveforms conveying no confidential information may also be exploited as the AN imposed on the communication signals for contaminating the eavesdropping channels. The main contributions of this paper are summarized as follows, and they are also boldly and explicitly contrasted to the literature at a glance in Table I.

- We develop jointly precoded communication and radar waveforms for secure transmission. Specifically, the AN of traditional PLS designs can be replaced by bespoke radar signals specifically designed for inflicting interference upon the Eves, whilst additionally increasing the DoF available for target detection.
- We formulate the joint beamforming design as a non-convex optimization problem under the consideration of both radar, communication and security performance. An SDR-based and the associated low complexity algorithms are also conceived for tackling the non-convexity of the problem, where we prove that the relaxation used in our scheme is tight.
- We propose a robust beamforming design for the more practical scenarios of imperfect estimations, including the uncertain target directions and the imperfect CSI acquired for the LUs. We also show that the globally optimal reconstruction method proposed for ideal scenarios still applicable to our robust beamforming scheme.
- We analyze the performance trade-offs among radar, communication and PLS both theoretically and by simulation for providing new insights into flexible beamforming.

Authorized licensed use limited to: UNIVERSITY OF SOUTHAMPTON. Downloaded on February 16,2023 at 09:13:26 UTC from IEEE Xplore. Restrictions apply.

TABLE II
FREQUENTLY USED SYMBOLS

Notation	Description
$\mathbf{R}$	Covariance matrix of the transmitted signals
$\mathbf{H}$	Communication CSI matrix
$\mathbf{W}_r$ ($\mathbf{W}_c$)	Radar (Communication) beamforming matrix
Γ_e (Γ_c)	SINR threshold at Eves (LUs)
K	Number of the LUs
Q	Number of the targets (Eves)
M	Number of antennas
β	Path-loss coefficient for radar channel
$L_r(\mathbf{R}, \alpha)$	Least square function for MIMO radar beampattern
γ_k ($\tilde{\gamma}_q$)	SINR of the k-th LU (the q-th Eve)

The rest of this paper is organized as follows. In Section II, we establish the mathematical model of joint communication and radar signal transmission and introduce the performance metrics of radar detection, multiuser communication, and system security, respectively. The proposed SDR-based beamforming and the low complexity ZF-based algorithms are characterized in Section III. Furthermore, Section IV provides our robust beamforming method relying on imperfect CSI knowledge, while the performance vs. the complexity of the proposed algorithms is analyzed in Section V. Finally, our simulation results and conclusions are provided in Sections VI and VII, respectively.

The notations used in this paper are as follows. Upper-case $\mathbf{A}$ (lower-case $\mathbf{a}$) bold characters denote matrices (column vectors), and lower case normal letters a are scalars; $(\cdot)^T$, $(\cdot)^*$ and $(\cdot)^H$ represent the transpose, conjugate and complex conjugate transpose operations respectively; $|a|$ and $\|\mathbf{a}\|_2$ stand for the magnitude of a scalar a and the ℓ_2-norm of the vector $\mathbf{a}$; $\mathbb{E}\{\cdot\}$ is the statistical expectation; diag$\{\mathbf{a}\}$ stands for a diagonal matrix using the elements of $\mathbf{a}$ as its diagonal elements; for a matrix $\mathbf{A}$, $[\mathbf{A}]_{[i,j]}$ denotes the (i, j)th element; $\mathbf{A}_{[:,1:k]}$ and $\mathbf{A}_{[1:k,:]}$ represent the sub-matrices containing the first k columns and rows of $\mathbf{A}$ respectively; $\mathbf{I}_M$ is the n-dimensional identity matrix and $\mathbf{0}_{M\times N}$ is the $M \times N$ matrix having all-zero entries. Frequently used symbols in this paper are summarized in Table II.

II. System Model and Performance Metrics

A. Transmission and Reception Signal Model

As shown in Fig. 1, a colocated MIMO BS transmits DFRC signals to detect Q targets and K LUs simultaneously. For the consideration of our PLS design, all the targets considered are non-cooperative, such as unmanned aerial vehicle (UAV) which are regarded as the potential Eves at the same time. We assume that the BS is equipped with M antennas arranged in a uniform linear array (ULA), and all the Eves and LUs have a single antenna. The proposed beamforming design can be readily extended to multi-antenna scenarios.

Following [13], the discrete-time transmitted signal at time slot n, which is the weighted sum of the communication signals and radar waveforms, can be expressed as

$$\mathbf{x}[n] = \mathbf{W}_r\mathbf{s}[n] + \mathbf{W}_c\mathbf{c}[n], n = 0, 1, \ldots, N-1, \tag{1}$$

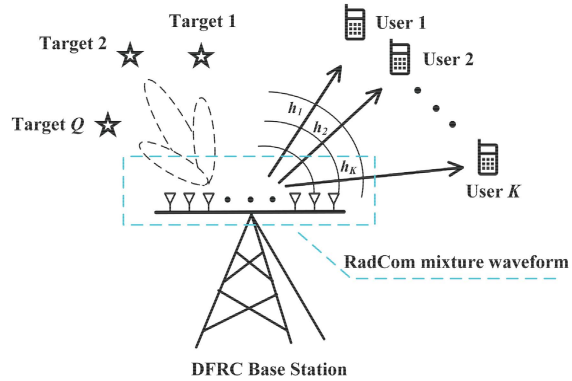

Fig. 1. The DFRC system detects the targets (Eves) and serves downlink users by transmitting mixture waveform.

where $\mathbf{s}[n] = [s_1[n], \ldots, s_M[n]]^T$ represents the individual radar signals and $\mathbf{c}[n] = [c_1[n], \ldots, c_K[n]]^T$ stands for the K parallel communication symbol streams intended for the LUs. N is the total number of symbols. Furthermore, $\mathbf{W}_r \in \mathbb{C}^{M\times M}$ and $\mathbf{W}_c \in \mathbb{C}^{M\times K}$ denote the beamforming matrices (or precoders) designed for the radar waveforms and communication waveforms. The conventional transmit signal strategy which only exploits the communication signals for detection in [10], [11], [12], [19], can be regarded as the special case associated with $\mathbf{W}_r = \mathbf{0}$. In line with the literature, the following assumptions are stipulated for the transmitted signals (1).

- Both the radar and communication signals have zero mean, and they are temporally white wide-sense stationary stochastic processes;
- The radar and the communication waveforms are statistically independent, hence we have $\mathbb{E}\{\mathbf{s}\mathbf{c}^H\} = \mathbf{0}_{M\times K}$;
- The M radar waveforms are orthogonal to each other, then we have $\mathbb{E}\{\mathbf{s}\mathbf{s}^H\} = \mathbf{I}_M$;
- The communication symbols transmitted to different LUs are uncorrelated, i.e., $\mathbb{E}\{\mathbf{c}\mathbf{c}^H\} = \mathbf{I}_K$;

Here, the signal power is normalized to unity. Thus, the covariance matrix of the transmitted signal can be written as

$$\mathbf{R} = \mathbb{E}\left\{\mathbf{x}\mathbf{x}^H\right\} = \mathbf{W}_r\mathbf{W}_r^H + \mathbf{W}_c\mathbf{W}_c^H. \tag{2}$$

Let $\mathbf{y} = [y_1, y_2, \ldots, y_K]^T$ denote the received signal vector of all the LUs, which can be expressed by

$$\mathbf{y} = \mathbf{H}\mathbf{x} + \mathbf{n}_c, \tag{3}$$

where $\mathbf{H} = [\mathbf{h}_1^*, \ldots, \mathbf{h}_K^*]^T \in \mathbb{C}^{K\times M}$ is the channel matrix and $\mathbf{h}_k$ represents the channel vector spanning from the BS to the kth LU, and $\mathbf{n}_c \sim \mathcal{CN}(0, \sigma_c^2\mathbf{I}_K)$ denotes the additive white Gaussian noise (AWGN). Moreover, the targets of interest can be viewed as virtual downlink users located in the LoS channel of DFRC systems [10]. Therefore, the signal received by the qth target (Eve) can be modeled as [19]

$$r_q = \beta_q\mathbf{a}^H(\theta_q)\mathbf{x} + n_e, \tag{4}$$

where β_q is the complex path-loss coefficient, n_e is the AWGN with covariance σ_e^2, and $\mathbf{a}(\theta)$ represents the ULA arrays' steering vector, which can be expressed as

$$\mathbf{a}(\theta) = \frac{1}{\sqrt{M}}\left[1, e^{\jmath 2\pi\frac{d}{\lambda}\sin(\theta)}, \ldots, e^{\jmath 2\pi(M-1)\frac{d}{\lambda}\sin(\theta)}\right]^T. \tag{5}$$

Authorized licensed use limited to: UNIVERSITY OF SOUTHAMPTON. Downloaded on February 16,2023 at 09:13:26 UTC from IEEE Xplore. Restrictions apply.

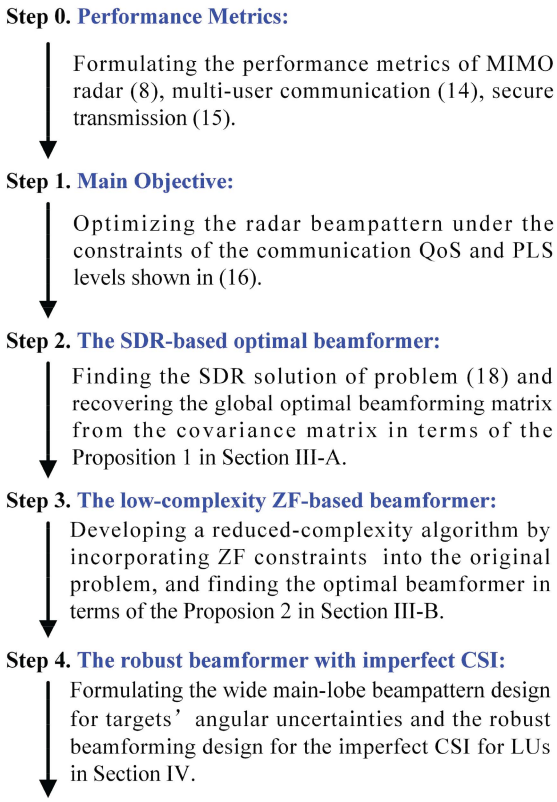

Fig. 2. Flow of the mathematical analysis.

Here, d is the antenna spacing, λ is the carrier wavelength, and θ is the azimuth of the target.

The BS has to acquire the CSI for both LUs and Eves before the beamforming design. In general, the CSI matrix $\mathbf{H}$ of LUs can be obtained through channel estimation and feedback techniques [21]. By contrast, the CSI from the BS to the Eve is challenging to acquire, since the Eves tend to be passive in general. Fortunately, the sensing functionality of the DFRC signal can be exploited for estimating the azimuth and path-loss coefficient through radar parameter estimation techniques [22], [23]. Since we only focus on the beamforming design, the processes of radar parameter estimation and information demodulation are ignored in this paper. The elaborate details can be found in [1], [24]. Before proceeding to our mathematical analysis, we have depicted in Fig. 2 the flow of the analysis described in the sequel, which allows readers to grasp the overall structure of this paper at a glance.

B. Performance Metrics

In our proposed physical layer beamformer designed for secure transmission, some important properties related to the symbol-level waveform design [11], [12] are not considered, such as the radar's ambiguity function, the peak-to-average power ratio (PAPR), etc. Next, we introduce our performance metrics used for the target detection, for the communication quality of service (QoS), and for the PLS level, respectively.

1) Performance Metric for MIMO Radar: In general, there are two primary MIMO radar functions, namely detection and tracking. MIMO radar tends to create both spatially orthogonal waveforms and omni-directional beampatterns (i.e., $\mathbf{R} = \mathbf{I}$) for detecting the potential targets in the detection stage, since there is no prior information concerning the targets. Then, in the tracking stage, MIMO radar steers the beam to the target directions of interest acquired during the previous observations. Instead of maximizing the SINR at radar receiver [25], we focus on the radar transmit beampattern performance. The synthesized radar beampattern at azimuth θ can be formulated as

$$P(\theta;\mathbf{R}) = \mathbb{E}\left\{\mathbf{a}^H(\theta)\mathbf{x}\mathbf{x}^H\mathbf{a}(\theta)\right\} = \mathbf{a}^H(\theta)\mathbf{R}\mathbf{a}(\theta). \tag{6}$$

Additionally, the cross-correlation pattern between direction θ_1 and θ_2 can be written as

$$P_c(\theta_1,\theta_2;\mathbf{R}) = \mathbf{a}^H(\theta_2)\mathbf{R}\mathbf{a}(\theta_1). \tag{7}$$

The objectives of beamformer design for MIMO radar include the following [26]

- Optimize the beampattern over the sectors of interest to concentrate the signal power while maintaining a low sidelobe level;
- Reduce the cross-correlation pattern over the set of target angles to achieve an excellent adaptive performance;

To this end, we adopt the loss function defined in terms of the least squares as our performance metric for MIMO radar, which is formulated as

$$L_r(\mathbf{R},\alpha) = L_b(\mathbf{R},\alpha) + \eta L_c(\mathbf{R}), \tag{8}$$

where η is the weighting factor representing the relative importance of the two terms based on the associated practical requirements. The first term represents the mean squared error between the designed and desired beampatterns, which can be formulated as

$$L_b(\mathbf{R},\alpha) = \frac{1}{L}\sum_{l=1}^{L}|\alpha\Phi(\theta_l) - P(\theta_l;\mathbf{R})|^2. \tag{9}$$

Here, α is a scaling factor, $\Phi(\theta)$ denotes the desired transmit beampattern, and $\{\theta_l\}_{l=1}^{L}$ represents the fine grid of points that cover the targets of interest. Let Δ denote the beam-width, then the desired beampattern at azimuth $\theta^\star$ is given by

$$\Phi(\theta) = \begin{cases} 1, \theta^\star - \frac{\Delta}{2} \le \theta \le \theta^\star + \frac{\Delta}{2} \\ 0, \text{otherwise.} \end{cases} \tag{10}$$

Moreover, the second term is the mean-squared cross-correlation pattern, given by

$$L_c(\mathbf{R}) = \frac{2}{P^2 - P}\sum_{p=1}^{P-1}\sum_{q=p+1}^{P}|P_c(\bar{\theta}_p,\bar{\theta}_q;\mathbf{R})|^2, \tag{11}$$

where $\{\theta_p\}_{p=1}^{P}$ are the given directions of the targets. We refer the reader to [13], [26] for more details.

2) Performance Metric for Multi-User Communication: The achievable transmission rate related to the SINR of the signal received by the downlink users is a standard performance measure in multiuser communication systems. For notation convenience, we introduce $\mathbf{W} = [\mathbf{W}_c, \mathbf{W}_r]$, where $\mathbf{w}_i$ is the

Authorized licensed use limited to: UNIVERSITY OF SOUTHAMPTON. Downloaded on February 16,2023 at 09:13:26 UTC from IEEE Xplore. Restrictions apply.

ith column of $\mathbf{W}$ for $i = 1, \ldots, K + M$. Then, the signal covariance matrix can be rewritten as

$$\mathbf{R} = \mathbf{W}\mathbf{W}^H = \sum_{i=1}^{K+M} \mathbf{w}_i \mathbf{w}_i^H = \sum_{i=1}^{K+M} \mathbf{R}_i, \tag{12}$$

where $\mathbf{R}_i = \mathbf{w}_i \mathbf{w}_i^H$ is the rank 1 covariance matrix. Specifically, $\mathbf{R}_1, \ldots, \mathbf{R}_K$ are the covariance matrices of communication symbols, where the last M ones are those of the radar waveforms. Thus, the SINR at the kth LU can be formulated as

$$\begin{aligned}\gamma_k &= \frac{\mathbb{E}\left\{|\mathbf{h}_k^H \mathbf{w}_k c_k|^2\right\}}{\sum_{i=1, i\neq k}^{K} \mathbb{E}\left\{|\mathbf{h}_k^H \mathbf{w}_i c_i|^2\right\} + \sum_{j=1}^{M} \mathbb{E}\left\{|\mathbf{h}_k^H \mathbf{w}_{j+K} s_j|^2\right\} + \sigma_c^2} \\ &= \frac{\mathbf{h}_k^H \mathbf{R}_k \mathbf{h}_k}{\sum_{i=1, i\neq k}^{K+M} \mathbf{h}_k^H \mathbf{R}_i \mathbf{h}_k + \sigma_c^2}.\end{aligned} \tag{13}$$

There are two popular design criteria for multiuser beamforming [27]. One of them is the throughput criterion to maximize the system's sum-rate. The other is the fairness criterion used for maximizing the minimal SINR at each user, which can be expressed as

$$\max \min\{\gamma_1, \ldots, \gamma_K\}. \tag{14}$$

In this work, the SINR-fairness is adopted as the performance metric for multiuser communication. On the one hand, the fairness metric guarantees that each LU can obtain satisfactory QoS. On the other hand, the fairness metric based optimization is more tractable than the NP-hard optimal throughput beamforming problem. Given a minimal level of communication QoS Γ_c, the SNR-fairness metric can be transformed to forcing the minimal SINR of the users to be higher than the target threshold, i.e., $\gamma_k \geq \Gamma_c, k = 1, \ldots, K$.

3) Performance Metric for PLS Level: When the targets become Eves, the achievable data rates at Eves are non-negligible. A straightforward method is to increase the proportion of interference signal power to the detriment of the useful signal. According to the previous analysis, the radar waveform conveying no desired information can be regarded as the interference contaminating the reception of Eves. Accordingly, by recalling the received signal model (4), the SINR for the qth Eve can be formulated as

$$\tilde{\gamma}_q = \frac{|\beta_q|^2 \mathbf{a}(\theta_q)^H \sum_{k=1}^{K} \mathbf{R}_k \mathbf{a}(\theta_q)}{|\beta_q|^2 \mathbf{a}(\theta_q)^H \sum_{i=K+1}^{K+M} \mathbf{R}_i \mathbf{a}(\theta_q) + \sigma_e^2}. \tag{15}$$

Following [19], we consider the worst-case SINR in (15), assuming that all the information intended for the K LUs is the desired signal for Eves. As stated in [28], there will exist modulation and coding schemes that allow the LUs rather than the Eves to reliably decode the transmit information, as long as $\gamma_k > \tilde{\gamma}_q$, for $\forall k, q$. Therefore, we restrict the maximal SINR at Eves to be less than a given threshold Γ_e, instead of optimizing the secrecy rate $[\log(1 + \gamma_k) - \log(1 + \tilde{\gamma}_q)]^+$ defined in [17], to achieve a satisfactory PLS level. On the one hand, the system's secrecy rate is difficult to determine due to its non-convexity with respect to $\mathbf{R}_i$. On the other hand, since SINR-fairness based schemes are still capable of maintaining a minimal communication rate due to the monotonicity of the log function, we can equivalently achieve a desired secrecy rate $[\log(1 + \Gamma_c) - \log(1 + \Gamma_e)]^+$ by appropriately choosing the thresholds Γ_c and Γ_e.

III. The Beamforming Design for Ideal Scenarios

In this section, we aim for designing the transmit beamforming matrices $\mathbf{W}_r$ and $\mathbf{W}_c$ under the consideration of the performance metrics for the radar beampattern, the communication QoS and the PLS levels given in the previous section. We first consider the ideal conditions, where the BS perfectly knows the CSI both for the LUs and Eves, and leave the beamformer design under the more practical imperfect CSI scenario for the next section.

A. The Proposed SDR-Based Beamforming Algorithm

Our beamforming design objective is to minimize the difference between the desired transmit beampattern and that generated by the BS to achieve good target detection and tracking performance. Meanwhile, the beamforming design also guarantees that the downlink SINR at the LUs remains higher than the given threshold, while that of the Eve is lower. Recalling the definition (12), instead of directly optimizing the precoding matrix $\mathbf{W}$, the SDR based optimization problem with respect to the variables $\mathbf{R}_i$ can be formulated as

$$\underset{\mathbf{R}, \{\mathbf{R}_i\}, \alpha}{\text{minimize}} \;\; L_r(\mathbf{R}, \alpha) (\mathcal{P}_0) \tag{$\mathcal{P}_0$}$$

$$\text{subject to} \;\; \mathbf{R} = \sum_{i=1}^{K+M} \mathbf{R}_i \in \mathcal{S}_M^+, \alpha > 0, \tag{16a}$$

$$\mathbf{R}_i \in \mathcal{S}_M^+, i = 1, \ldots, K + M, \tag{16b}$$

$$\text{rank}(\mathbf{R}_i) = 1, i = 1, \ldots, K + M, \tag{16c}$$

$$[\mathbf{R}]_{[m,m]} = P_t/M, m = 1, \ldots, M, \tag{16d}$$

$$\gamma_k \geq \Gamma_c, k = 1, \ldots, K, \tag{16e}$$

$$\tilde{\gamma}_q \leq \Gamma_e, q = 1, \ldots, Q, \tag{16f}$$

where $\mathcal{S}_M^+$ represents the set consisting of all M-dimensional complex positive semidefinite matrices, i.e., $\mathcal{S}_M^+ = \{\mathbf{A} | \mathbf{A} \in \mathbb{C}^{M\times M}, \mathbf{A} = \mathbf{A}^H, \mathbf{A} \succeq 0\}$. The rank-1 constraint in (16c) is equivalent to $\mathbf{R}_i = \mathbf{w}_i \mathbf{w}_i^H$. (16d) represents the per-antenna power constraints, and P_t is the total transmit power of the BS. Furthermore, the objective function and the constraints (16e), (16f) are the performance metrics introduced in Section II-B, where Γ_c and Γ_e are the predefined SINR thresholds at the LUs and Eve, respectively.

Upon substituting the SINR expressions (13) as well as (15) into the constraints and applying some simple mathematical manipulations, (16e) and (16f) can be recast as

$$\left(1 + \Gamma_c^{-1}\right) \mathbf{h}_k^H \mathbf{R}_k \mathbf{h}_k \geq \mathbf{h}_k^H \mathbf{R} \mathbf{h}_k + \sigma_c^2, \forall k \tag{17a}$$

$$\left(1 + \Gamma_e^{-1}\right) \mathbf{a}_q^H \sum_{k=1}^{K} \mathbf{R}_k \mathbf{a}_q \leq \mathbf{a}_q^H \mathbf{R} \mathbf{a}_q + \frac{\sigma_e^2}{|\beta_q|^2}, \forall q \tag{17b}$$

where $\mathbf{a}_q$ is the abbreviated form of $\mathbf{a}(\theta_q)$. It can be observed that the individual matrices $\{\mathbf{R}_i\}_{i\geq K+1}$ have no effect on the SINR constraints, which motivates us to remove these matrix

Authorized licensed use limited to: UNIVERSITY OF SOUTHAMPTON. Downloaded on February 16,2023 at 09:13:26 UTC from IEEE Xplore. Restrictions apply.

variables from the original problem $\mathcal{P}_0$ of (16). As a result, the number of matrix variables is reduced from $K+M+1$ to $K+1$, leading to much reduced memory requirements. By reformulating the constraint (16a), problem $\mathcal{P}_0$ can be transformed to

$$\underset{\mathbf{R},\mathbf{R}_1,\ldots,\mathbf{R}_K,\alpha}{\text{minimize}} \quad L_r(\mathbf{R},\alpha) \qquad (\mathcal{P}_1)$$

$$\text{subject to} \quad \mathbf{R}\in\mathcal{S}_M^+,\ \mathbf{R}-\sum_{k=1}^{K}\mathbf{R}_k\in\mathcal{S}_M^+, \qquad (18a)$$

$$\alpha>0, \mathbf{R}_k\in\mathcal{S}_M^+, k=1,\ldots,K, \qquad (18b)$$

$$\text{rank}(\mathbf{R}_k)=1, k=1,\ldots,K, \qquad (18c)$$

$$[\mathbf{R}]_{[m,m]}=P_t/M, m=1,\ldots,M, \qquad (18d)$$

$$(17a),\ (17b).$$

However, problem $\mathcal{P}_1$ is non-convex due to the rank-1 constraints. Thus, the SDR relaxation based version of problem $\mathcal{P}_1$ can be obtained by omitting the rank-1 constraints (18c), which is denoted by problem $\mathcal{P}_2$. Thus, the problem $\mathcal{P}_2$ has become a standard quadratic semidefinite program (QSDP), since the objective function is a positive-semidefinite quadratic form and all the constraints are either linear or semidefinite. Hence, the global optimum can be obtained in polynomial time with the aid of standard convex optimization toolboxes [29], [30]. Note that the optimal solutions of the relaxed problem $\mathcal{P}_2$ are not necessarily rank-1 matrices, hence either the classic eigenvalue decomposition or Gaussian randomization methods [31] can be leveraged to obtain the solutions of the original problem $\mathcal{P}_1$. Unfortunately, these kinds of approximate algorithms usually only provide suboptimal solutions of the original problem, hence resulting in a loss of performance.

To circumvent this deficiency, we set out to find a global optimum for problem $\mathcal{P}_1$, which means that the SDR relaxation is tight. Inspired by the result in [13], we propose the following proposition.

Proposition 1: Let $\hat{\mathbf{R}},\hat{\mathbf{R}}_1,\ldots,\hat{\mathbf{R}}_K$ be the optimal solution of the QSDP problem $\mathcal{P}_2$. There also exists a global optimum $\tilde{\mathbf{R}},\tilde{\mathbf{R}}_1,\ldots,\tilde{\mathbf{R}}_K$ for problem $\mathcal{P}_1$, where we have

$$\tilde{\mathbf{R}}=\hat{\mathbf{R}}, \tilde{\mathbf{w}}_k=\left(\mathbf{h}_k^H\hat{\mathbf{R}}_k\mathbf{h}_k\right)^{-1/2}\hat{\mathbf{R}}_k\mathbf{h}_k, \tilde{\mathbf{R}}_k=\tilde{\mathbf{w}}_k\tilde{\mathbf{w}}_k^H, \quad (19)$$

for $k=1,\ldots,K$.

Proof: The proof is relegated to Appendix A. ■

According to Proposition 1, we can get the global rank-1 optimal solution for problem $\mathcal{P}_1$ from its QSDP relaxation based version $\mathcal{P}_2$, where the relaxation is tight. The remaining step is to find the optimal solution for the original problem $\mathcal{P}_0$, i.e., obtaining the precoding matrix $\mathbf{W}_r$ for the radar waveforms. To meet the constrains of (16a) and (16b), the M precoding vectors $\{\mathbf{w}_i\}_{i\geq K+1}$ can be obtained by the following decomposition

$$\mathbf{W}_r\mathbf{W}_r^H=\mathbf{R}_{\text{rad}}=\tilde{\mathbf{R}}-\sum_{k=1}^{K}\tilde{\mathbf{R}}_k, \qquad (20)$$

where $\mathbf{W}_r=[\mathbf{w}_{K+1},\ldots,\mathbf{w}_{K+M}]$. Actually, since the associated waveform level design is not considered in this work, the decomposition (20) is not unique, but it is trivial thanks to the positive semi-definite nature of the radar signal's covariance matrix. Several decomposition methods such as the square root matrix ($\mathbf{W}_r=\mathbf{R}_{\text{rad}}^{\frac{1}{2}}\mathbf{U}$, $\mathbf{U}$ is an arbitrary unitary matrix) based one [32] and the Cholesky decomposition based one may be applied [33].

B. The ZF-Based Low Complexity Algorithm

The main computational complexity burden in the proposed SDR-based algorithm is imposed by that of solving the QSDP problem $\mathcal{P}_2$, which motivates us to seek a low-complexity solution. Inspired by the zero forcing (ZF) based method of [13], we develop a reduced-complexity sub-optimal algorithm by incorporating ZF constraints into problem $\mathcal{P}_2$. The ZF method is widely used in low-complexity linear precoders, because its performance tends to that of the optimal non-linear precoder, especially for a large number of antennas [34], [35]. Its main appeal is that of eliminating the inter-user and radar interferences, hence achieving a high SINR at each user. Mathematically, the ZF constraints can be expressed as

$$\mathbf{H}\mathbf{W}_c=\text{diag}(\sqrt{\rho_1},\ldots,\sqrt{\rho_K}), \mathbf{H}\mathbf{W}_r=\mathbf{0}_{K\times M}, \quad (21)$$

where ρ_k represents the signal power at the kth user, for $1\leq k\leq K$. Upon recalling the definition $\mathbf{W}=[\mathbf{W}_c,\mathbf{W}_r]$ and $\mathbf{R}=\mathbf{W}\mathbf{W}^H$, (21) can be equivalently transformed to the following form [13, Th. 2]

$$\mathbf{H}\mathbf{R}\mathbf{H}^H=\text{diag}(\boldsymbol{\rho}), \qquad (22)$$

where $\boldsymbol{\rho}=[\rho_1,\ldots,\rho_K]$. Moreover, substituting (21) or (22) into the SINR expression (13), the associated SINR constraints (17a) can be simplified by

$$\rho_k\geq\Gamma_c\sigma_c^2, \forall k. \qquad (23)$$

It can be observed that the individual matrix variable $\mathbf{R}_k$ has been removed from the SINR constraints for the LUs by imposing the ZF constraints. Following the same methodology for further reducing the number of matrix variables, and by introducing the auxiliary matrix variable $\mathbf{R}_{\text{com}}=\sum_{k=1}^{K}\mathbf{R}_k$, the PLS constraint (17b) can be rewritten as follows

$$\left(1+\Gamma_e^{-1}\right)\mathbf{a}_q^H\mathbf{R}_{\text{com}}\mathbf{a}_q\leq\mathbf{a}_q^H\mathbf{R}\mathbf{a}_q+\frac{\sigma_e^2}{|\beta_q|^2}, \forall q \qquad (24)$$

Furthermore, we can immediately infer the ZF constraint for $\mathbf{R}_{\text{com}}$ as

$$\mathbf{H}\mathbf{R}_{\text{com}}\mathbf{H}^H=\mathbf{H}\mathbf{W}_c\mathbf{W}_c^H\mathbf{H}^H=\text{diag}(\boldsymbol{\rho}). \qquad (25)$$

As a consequence, either the communication SINR constraint or the PLS constraint no longer contains the individual matrix variable $\mathbf{R}_k$. Accordingly, problem $\mathcal{P}_2$ can be converted to

$$\underset{\mathbf{R},\mathbf{R}_{\text{com}},\boldsymbol{\rho},\alpha}{\text{minimize}} \quad L_r(\mathbf{R},\alpha) \qquad (\mathcal{P}_3)$$

$$\text{subject to} \quad \mathbf{R}\in\mathcal{S}_M^+, \mathbf{R}-\mathbf{R}_{\text{com}}\in\mathcal{S}_M^+, \mathbf{R}_{\text{com}}\in\mathcal{S}_M^+, \quad (26a)$$

$$[\mathbf{R}]_{[m,m]}=P_t/M, m=1,2,\ldots,M, \qquad (26b)$$

$$\mathbf{H}\mathbf{R}\mathbf{H}^H=\text{diag}(\boldsymbol{\rho}), \qquad (26c)$$

Authorized licensed use limited to: UNIVERSITY OF SOUTHAMPTON. Downloaded on February 16,2023 at 09:13:26 UTC from IEEE Xplore. Restrictions apply.

$$\mathbf{H}\mathbf{R}_{\text{com}}\mathbf{H}^H = \text{diag}(\boldsymbol{\rho}),$$
$$\alpha > 0,\ (23),\ (24). \tag{26d}$$

Problem $\mathcal{P}_3$ is also a standard QSDP problem, because the objective function has a positive-semidefinite quadratic form and all the constraints are either linear or semidefinite. Similarly, the optimal solutions $\hat{\mathbf{R}}$ and $\hat{\mathbf{R}}_{\text{com}}$ can be obtained by a standard convex optimization toolbox in polynomial time.

The next step is to recover the precoding matrix $\mathbf{W}$ from the optimal solutions $\hat{\mathbf{R}}$ and $\hat{\mathbf{R}}_{\text{com}}$. Inspired by [13, Th. 2], we conceive the following procedure of constructing the radar and communication precoding matrices, respectively. First, either the classic Cholesky decomposition or square root method is used by exploiting the positive-semidefinite property for $\hat{\mathbf{R}}_{\text{com}} = \mathbf{L}_c\mathbf{L}_c^H$. Then, we employ the row QR decomposition of $\mathbf{H}\mathbf{L}_c$, yielding

$$\mathbf{H}\mathbf{L}_c = \left[\mathbf{L}_h, \mathbf{0}_{K\times(M-K)}\right]\mathbf{Q}, \tag{27}$$

where $\mathbf{L}_h$ is a $K \times K$ lower triangular matrix and $\mathbf{Q}$ is a $M \times M$ unitary matrix. Thus, the communication precoder can be formulated as

$$\mathbf{W}_c = \mathbf{L}_c\left[\mathbf{Q}^H\right]_{[:,1:K]}, \tag{28}$$

while the radar precoding matrix $\mathbf{W}_r$ can be expressed as

$$\mathbf{W}_r\mathbf{W}_r^H = \hat{\mathbf{R}}_{\text{rad}} = \hat{\mathbf{R}} - \mathbf{W}_c\mathbf{W}_c^H. \tag{29}$$

Subsequently, we analyze the feasibility of the proposed precoder design method by introducing the following proposition.

Proposition 2: Given the optimal solution $\hat{\mathbf{R}}$ and $\hat{\mathbf{R}}_{\text{com}}$ of problem $\mathcal{P}_3$, the matrices $\mathbf{W}_c$ in (28) and $\mathbf{W}_r$ in (29) are also the optimal precoders of problem $\mathcal{P}_3$ and satisfy the ZF constraint (21) at the same time.

Proof: The proof is divided into three parts, and it is relegated to Appendix B. ■

Proposition 2 illustrates the feasibility and efficiency of the proposed precoding matrices recovered from the optimal solution of problem $\mathcal{P}_3$. In summary, we can obtain the optimal beamforming for DFRC secure transmission with the perfectly known CSI by the proposed SDR-based and the low complexity ZF-based algorithms. The detailed procedure of the proposed algorithms are summarized in Algorithm 1.

Algorithm 1 The Proposed SDR(ZF)-Based Beamforming Algorithm Designed for Secure DFRC

Input:
Total transmit power of base station P_t;
Radar desired beampattern $\Phi(\theta)$;
Instantaneous downlink channel $\mathbf{H}$;
SINR threshold at LUs Γ_c and at Eves Γ_e;
The directions of Eves $\theta_q, q = 1, \ldots, Q$;
Output
The overall precoding matrix $\mathbf{W} = [\mathbf{w}_1, \ldots, \mathbf{w}_{K+M}]$.
Steps
1. Compute the optimal solution of $\mathcal{P}_2$ (or $\mathcal{P}_3$) via convex optimization solver;
2. Compute $\mathbf{w}_1, \ldots, \mathbf{w}_K$ by (19) (or by (28));
3. Compute $\mathbf{w}_{K+1}, \ldots, \mathbf{w}_{K+M}$ by (20) (or by (29));

IV. Robust Beamforming Design With Imperfect CSI Knowledge

In practice, it is challenging to obtain the exact CSI due to the estimation errors, feedback quantization, hardware deficiencies, etc., resulting in imperfect CSI knowledge at the BS. Specifically, for the radar targets, we assume that the direction of the q-th target is roughly known by the BS within an angular interval of $[\theta_q - \Delta\theta_q, \theta_q + \Delta\theta_q]$, where $\Delta\theta_q$ represents the associated angle uncertainty. Moreover, for the communication LUs, the additive error model of the CSI matrix for the k-th LU is considered as $\mathbf{h}_k = \hat{\mathbf{h}}_k + \boldsymbol{\epsilon}_k$, where $\hat{\mathbf{h}}_k$ is the estimated CSI matrix and $\boldsymbol{\epsilon}_k$ denotes the channel uncertainty. To this end, we aim for designing the robust beamforming scheme for secure transmission in this section.

A. Wide Main-Lobe Beampattern Design

The uncertainties of the target directions have an impact on both the objective function and the PLS constraints in problem $\mathcal{P}_0$. On one hand, the BS should form a wide main-lobe to avoid missing the target. Thus, the beam-width Δ in (10) should be appropriately chosen according to the angular uncertainty $\Delta\theta_q$, in order to cover all the possible locations of the target.

On the other hand, since Eve may be located in an arbitrary direction within the angular interval, we should guarantee a satisfactory secrecy rate for every possible direction. Consequently, the SINR constraints (17b) should be modified according to

$$\left(1 + \Gamma_e^{-1}\right)\mathbf{a}_{q_i}^H \sum_{k=1}^{K} \mathbf{R}_k\mathbf{a}_{q_i} \le \mathbf{a}_{q_i}^H\mathbf{R}\mathbf{a}_{q_i} + \frac{\sigma_e^2}{|\beta_q|^2}, \forall\theta_{q_i} \in \bar{\Omega}_q, \tag{30}$$

where $\bar{\Omega}_q$ is a discrete set that covers the potential directions of the q-th Eve, and $\mathbf{a}_{q_i}$ represents the compact form of $\mathbf{a}(\theta_{q_i})$. It can be observed that the angular uncertainty introduces more constraints similar to (17b) over the associated angular interval. Evidently, the proposed Algorithm 1 is also capable of handling the modified constraints (30). In other words, the number of targets and the uncertainty of target directions determine the number of PLS constraints. Naturally, imposing a large number of constraints for securing certain PLS levels results in degraded radar beampattern and communication QoS. We will illustrate this phenomenon in Section VI.

B. Robust Beamforming for Mitigating CSI Error of LUs

Similar to [19], [37], we assume that the CSI uncertainty is bounded by a spherical region as

$$\mathcal{S}_k := \left\{\hat{\mathbf{h}}_k + \boldsymbol{\epsilon}_k \middle| \|\boldsymbol{\epsilon}_k\| \le u_k\right\}, \forall k. \tag{31}$$

In this case, the SINR expression for the k-th LU in (13) should be replaced by the worst-case SINR over the set $\mathcal{S}_k$, namely

$$\bar{\gamma}_k = \min_{\mathbf{h}_k \in \mathcal{S}_k} \gamma_k, \forall k. \tag{32}$$

Authorized licensed use limited to: UNIVERSITY OF SOUTHAMPTON. Downloaded on February 16,2023 at 09:13:26 UTC from IEEE Xplore. Restrictions apply.

Thus, based on the definitions (31) and (32), the SINR constraint in (17a) can be reformulated as

$$\left(\hat{\mathbf{h}}_k+\boldsymbol{\epsilon}_k\right)^H\left[\left(1+\Gamma_c^{-1}\right)\mathbf{R}_k-\mathbf{R}\right]\left(\hat{\mathbf{h}}_k+\boldsymbol{\epsilon}_k\right)-\sigma_c^2\geq 0,\forall k. \tag{33}$$

Then, we adopt the popular S-procedure of robust optimization to tackle the SINR constraints mentioned above. By introducing an auxiliary vector $\mathbf{t}=[t_1,\ldots,t_K]$, the original problem $\mathcal{P}_1$ can be reformulated as the following robust beamforming version [19], [37]

$$\underset{\mathbf{R},\mathbf{R}_1,\ldots,\mathbf{R}_K,\mathbf{t},\alpha}{\text{minimize}} \quad L_r(\mathbf{R},\alpha) \tag{$\mathcal{P}_4$}$$

$$\begin{aligned}\text{subject to}\ \ &(18a)-(18d),\ (17b)\text{ or }(30),\\ &\begin{pmatrix}\mathbf{S}_k+t_k\mathbf{I}_M & \mathbf{S}_k\hat{\mathbf{h}}_k\\ \hat{\mathbf{h}}_k^H\mathbf{S}_k & \mathbf{h}_k^H\mathbf{S}_k\mathbf{h}_k-\sigma_c^2-t_ku_k^2\end{pmatrix}\succeq 0,\forall k\\ &\mathbf{S}_k:=\left(1+\Gamma_c^{-1}\right)\mathbf{R}_k-\mathbf{R},t_k\geq 0.\end{aligned} \tag{34}$$

Again, by dropping the rank-1 constraints (18c), problem $\mathcal{P}_4$ becomes a QSDP, which can be efficiently solved in polynomial time. Then, we will show that the optimal solution of the QSDP reconstruction method in (19) also holds for the proposed robust beamforming.

Proposition 3: Let $\hat{\mathbf{R}},\hat{\mathbf{R}}_1,\ldots,\hat{\mathbf{R}}_K$ be the optimal solution of the relaxed version of problem $\mathcal{P}_4$. Then the $\tilde{\mathbf{R}},\tilde{\mathbf{R}}_1,\ldots,\tilde{\mathbf{R}}_K$ associated with the expression of (19) is also the optimal solution of the original problem $\mathcal{P}_4$.

Proof: By employing the result in Proposition 1, the proof becomes straightforward upon substituting (19) into the constraints (33). ■

V. Performance and Complexity Analysis

A. Complexity Analysis

The complexity of the proposed algorithms is dominated by the QSDP problem. For a given solution accuracy ϵ, the worst-case complexity order of solving problem $\mathcal{P}_2$ using the primal-dual interior-point algorithm is $\mathcal{O}[(K+Q)^{6.5}M^{6.5}\log(1/\epsilon)]$ [13], [38], where $K+Q$ and M refer to the number of semidefinite constraints and the dimension of matrix variables, respectively. Compared to the SDR algorithm, the low complexity ZF beamforming problem $\mathcal{P}_3$ includes $5=\mathcal{O}(1)$ such constraints, hence the worst-case complexity order becomes $\mathcal{O}[Q^{6.5}M^{6.5}\log(1/\epsilon)]$. Furthermore, for the robust beamforming algorithm with imperfect CSI knowledge, the complexity also depends on the number of elements in the set $\bar{\Omega}_q$ of (30). Specifically, upon denoting the cardinality of the set $\bar{\Omega}_q$ as P, the worst-case complexity is on the order of $\mathcal{O}[K^{6.5}P^{6.5}M^{6.5}\log(1/\epsilon)]$.

B. Performance Analysis

In this subsection, we provide the performance analysis of the proposed algorithms.

(I) We can immediately spot the performance trade-off among the radar beampattern, the communication QoS, and the PLS level in problem $\mathcal{P}_1$. The constraints (17a) and (17b) always hold, when we have $\Gamma_c=0$ and $\Gamma_e\to\infty$. In this case, problem $\mathcal{P}_1$ is reduced to the conventional radar-only beamforming design, determining the optimal beampattern for radar detection. Explicitly, any improvements of the communication QoS and PLS level are attained at the cost of sacrificing the radar performance, since the radar loss function will increase upon increasing Γ_c or decreasing Γ_e.

(II) Compared to the SDR-based algorithm, the low complexity ZF-based algorithm forces the radar and inter-user interference to zero, potentially raising the SINR at the LUs to a certain threshold (denoted by $\hat{\Gamma}$). Thus, for the communication constraints, we have

$$\begin{cases}\gamma_k^{\text{ZF}}=\hat{\Gamma}>\gamma_k^{\text{SDR}}\geq\Gamma_c,\text{when}\Gamma_c<\hat{\Gamma},\\ \gamma_k^{\text{ZF}}=\gamma_k^{\text{SDR}}\geq\Gamma_c\geq\hat{\Gamma},\text{when}\Gamma_c\geq\hat{\Gamma}.\end{cases} \tag{35}$$

For a relatively low threshold Γ_c, the interference encountered by the users do not have to be as low as zero to satisfy the SINR constraint, resulting in $\gamma_k^{\text{ZF}}>\gamma_k^{\text{SDR}}$. By contrast, the interference in γ_k^{SDR} has to be eliminated to meet the high SINR requirements, resulting in $\gamma_k^{\text{ZF}}=\gamma_k^{\text{SDR}}$. According to (35), we can immediately conclude the following properties of the ZF-based algorithm. (1) It results in worse radar beampattern than the SDR-based algorithm because more severe restrictions are imposed by the ZF constraint when $\Gamma_c<\hat{\Gamma}$. (2) The radar loss function and the users' SINR remains constant, as long as the threshold Γ_c is lower than a positive value $\hat{\Gamma}$. (3) The performance of ZF-based beamforming tends to be similar to that of SDR-based beamforming at high SINRs, i.e., $\Gamma_c\geq\hat{\Gamma}$.

(III) For the SDR-based algorithm, the system's secrecy rate is always approximated by $\log_2(1+\Gamma_c)-\log_2(1+\Gamma_e)$ given the thresholds Γ_c and Γ_e, because the optimal solution generally reaches the boundary of the feasible region. By contrast, the secrecy rate of the ZF-based algorithm may become higher than the above value for small Γ_c values due to the potentially high SINR achieved under the ZF constraint. The proposed algorithms guarantee to have a secrecy rate above a certain lower bound.

(IV) Upon considering the extreme case that the channels of the users and Eves have the same quality, i.e., $\beta_k\mathbf{a}(\theta_k)=\mathbf{h}_k$, the communication QoS constraint (17a) and the PLS level constraint (17b) are contradictory to each other, hence leading to the infeasibility of problem $\mathcal{P}_1$. This means that the feasibility probability of problem $\mathcal{P}_1$ significantly depends on the values of Γ_c as well as Γ_e, and on the distances between the targets and Eves. The proposed joint beamforming design method will become invalid, when the Eves are at the same directions as the users. The symbol-level range sidelobe design [36] may be a promising remedy, which we will leave for future research.

(V) It should be pointed out that the joint PLS beamforming design of [19] minimized the SINR at Eve, which is different from the proposed method optimizing the radar transmit beampattern. Even though it cannot be compared directly due to the different functional requirements, the proposed method has the following advantages over [19]. (1) The fractional programming approach is adopted in [19], where a sequence of SDPs has to be solved by iteration, imposing a heavy computational burden. By contrast, the proposed methods only have to

Authorized licensed use limited to: UNIVERSITY OF SOUTHAMPTON. Downloaded on February 16,2023 at 09:13:26 UTC from IEEE Xplore. Restrictions apply.

solve a SDP or QSDP problem with the same number of matrix variables. (2) The eigenvalue decomposition or Gaussian randomization techniques of [19] result in a sub-optimal solution, when the ranks of the optimal matrices obtained by the SDP solver are not equal to 1. By contrast, the proposed SDR relaxation is tight. (3) When using the SINR instead of the secrecy rate as the objective, the difference between the achievable rate of users and that of Eves may become negative, leading to a secrecy rate of SR $= 0$. By contrast, the proposed algorithms can always guarantee a satisfactory secrecy rate.

VI. Simulation Results

In this section, we evaluate the proposed joint PLS beamforming algorithm by numerical simulations. The system parameters are set as follows, unless specified otherwise. The BS is equipped with a ULA having half-wavelength spacing between adjacent antennas, i.e., $d/\lambda = 1/2$. The number of antennas is set to $M = 10$, and the total transmit power is normalized as $P_t = 1$. The angular directions are obtained by uniform sampling with resolution of $0.1°$, including $\{\theta_l\}_{l=1}^{L}$ in (9) with the range of $[-90°, 90°]$, and Ω_q in (30). Without loss of generality, we adopt the Rayleigh fading model for the multi-user communication channel so that each entry of $\mathbf{H}$ obeys the standard complex Gaussian distribution with $h_{i,j} \sim \mathcal{CN}(0,1)$. Additionally, we assume the noise levels at the Eves and LUs to be the same, i.e., $\sigma_c^2 = \sigma_e^2 = 0.01$ for convenience. The individual radar waveforms and communication symbols are generated as random quadrature-phase-shift-keying (QPSK) modulated sequences, with the total number of symbols being $N = 1024$.

For comparison, we choose the joint beamforming design method and its low-complexity counterpart proposed in [13] termed as *Benchmark 1* and *Benchmark 2*, respectively. Compared to [10], where only the communication signal is exploited by the DFRC system, the superiority of the combined radar waveforms and communication signals in terms of increasing the DoFs has been shown in [13]. Therefore, we refer to [13] for circumventing repetition.

First, we numerically characterize the MIMO radar transmit beampattern, where the proposed SDR-based algorithm and its low-complexity version are referred to as SDR and ZF, respectively. We set the direction of a single target to $\theta_0 = 0°$, the threshold for the LUs' SINRs to $\Gamma_c = 10$ dB, and the threshold for the Eve's SINR to $\Gamma_e = 0$ dB. Fig. 3 illustrates the trade-off among the radar beampattern, the communication QoS and the PLS level. Although the proposed algorithms impose a performance degradation on the transmit beampattern compared to their counterparts, the target secrecy rate (SR) can still be guaranteed. By contrast, *Benchmark* 1 and 2 form better beampatterns, but their SR becomes zero. Then, we evaluate the system performance versus the predefined SINR thresholds Γ_c and Γ_e, respectively.

A. System Performance Evaluation vs. the Threshold Γ_c

In this subsection, we keep the SINR threshold of Eves $\Gamma_e = 0$ dB as a constant, and sweep Γ_c of LUs from 10dB to 18dB to test its impact. All of the simulation results represent averaged values over 500 Monte Carlo trials. In each trial, the target direction θ_q is chosen randomly in the range of $[-60°, 60°]$, and the CSI of the link spanning from the BS and the LUs obey the standard Complex Gaussian distribution. The radar performance is evaluated as the difference between the DFRC transmit beampattern and the optimal radar-only beampattern by defining the mean square error (MSE) metric as

$$\mathrm{MSE} = \frac{1}{L}\sum_{l=1}^{L} |P\left(\theta_l; \hat{\mathbf{R}}\right) - P(\theta_l; \mathbf{R}^\star)|^2, \tag{36}$$

where $\mathbf{R}^\star$ is the optimal radar-only variance matrix by the 3dB low sidelobe beampattern design scheme of [26].

Fig. 4 shows the beampattern MSE versus the SINR threshold Γ_c of the LUs. We can observe the following three phenomena from Fig. 4. (1) The beampattern MSEs of all algorithms increase upon increasing Γ_c, which is consistent with the previous analysis. As expected, the MSE of the ZF-based algorithms remains constant in the scenarios of $K = 2$ and for SINRs below 16dB at $K = 4$. This is because the ZF-based methods force the interference to zero, leading to a potentially high SINR. Thus, the performance will remain constant until the SINR thresholds become higher than the potential SINR achieved by the ZF constraint. The performance gaps between the SDR-based and ZF-based methods become quite small for high enough values of Γ_c. (2) The benchmark algorithms formulate better beampattern, since the PLS aspects of confidential information protection is not taken

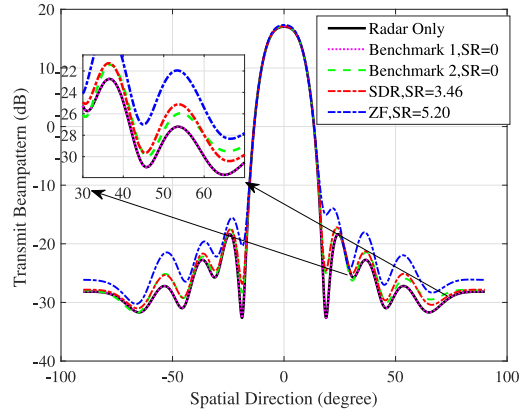

Fig. 3. Radar transmit beampattern for the direction $\theta_0 = 0°$, with $K = 2$, $\Gamma_c = 10$ dB, and $\Gamma_e = 0$ dB.

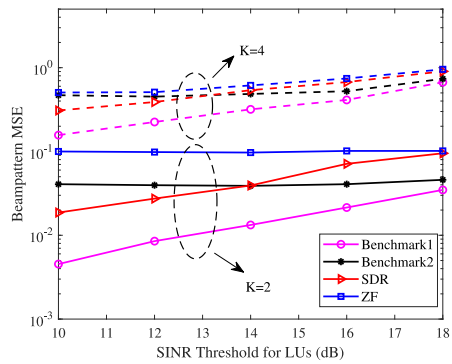

Fig. 4. Beampattern MSE versus SINR threshold Γ_c for LUs, $\Gamma_e = 0$ dB.

Authorized licensed use limited to: UNIVERSITY OF SOUTHAMPTON. Downloaded on February 16,2023 at 09:13:26 UTC from IEEE Xplore. Restrictions apply.

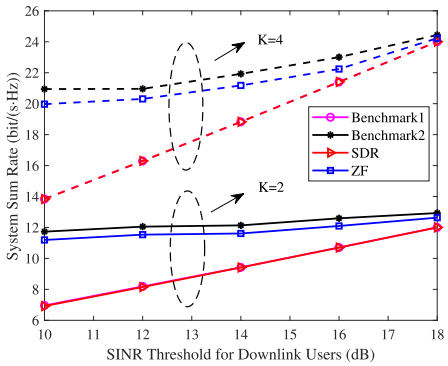

Fig. 5. The achievable sum rate versus SINR threshold Γ_c for LUs, $\Gamma_e = 0$ dB.

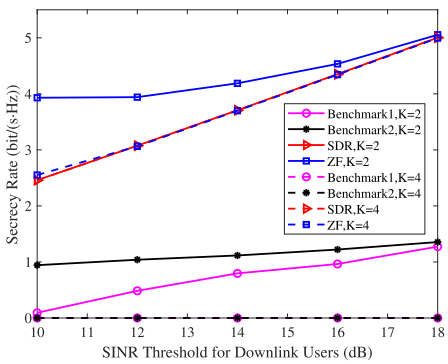

Fig. 6. The secrecy rate versus SINR threshold Γ_c for LUs, $\Gamma_e = 0$ dB.

into account in these methods. (3) The more users have to be supported, the higher the beampattern MSE becomes. Notably, the impact of the number of users K on the beampattern MSE is more significant than that of the SINR threshold Γ_c, which implies that serving more downlink users is more restrictive than improving the SINR level of the users.

In Fig. 5, we quantify the achievable sum-rate versus the SINR threshold Γ_c, where the system sum-rate is defined by $\sum_{k=1}^{K} \log_2(1+\gamma_k)$. The SDR and *Benchmark 1* curves are fairly similar and increase linearly with the SINR constraint Γ_c. This is because the optimal solution should reach the SINR boundary related to the given threshold. Conversely, as seen in the analysis of Section V-B, the ZF-based beamformer achieves a higher communication sum rate to the detriment of the radar performance. Meanwhile, the performances of the SDR-based and ZF-based beamformer tend to become similar at high SINR thresholds for both $K = 2$ and 4. Furthermore, the curves of the *Benchmark* 2 are slightly higher than those of the proposed ZF algorithms, since there is an additional minimum PLS constraint imposed on the ZF algorithm.

Fig. 6 illustrates the system's secrecy rate versus the SINR threshold Γ_c. Observe that the curves of SDR associated with $K = 2$ and $K = 4$ are coincident and increase linearly upon increasing Γ_c. Recall from Section V-B that the system's secrecy rate will only reach the value of $\log_2(1+\Gamma_c) - \log_2(1+\Gamma_e)$, if the optimization problem is feasible, regardless of how the other parameters change. Additionally, the ZF-based beamformer associated with $K = 2$ achieves a higher

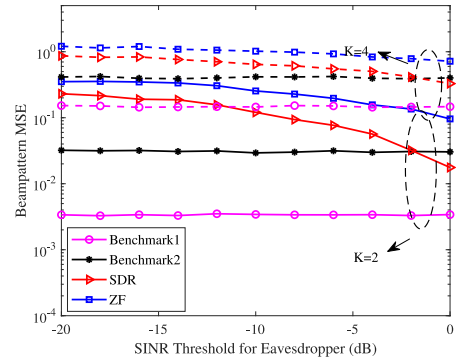

Fig. 7. Beampattern MSE versus SINR threshold Γ_e for Eves, $\Gamma_c = 10$ dB.

secrecy rate than that of the SDR-based algorithm at small values of Γ_c, since it can reach a higher SINR level than the given threshold. However, the secrecy rate of these two algorithms becomes similar for $K = 4$. Actually, supporting more communication users imposes more restrictions on the optimization problem $\mathcal{P}_3$, hence forcing the minimal SINR level to approximate the threshold Γ_c. Moreover, the proposed PLS-protected beamforming design guarantees a satisfactory PLS level by appropriately choosing the thresholds. By contrast, the benchmark 1 and 2 are not capable of secrecy protection, especially not for numerous legitimate users K.

B. System Performance Evaluation vs. the Threshold Γ_e

In this subsection, we evaluate the system performance versus the SINR threshold Γ_e of the Eves. Accordingly, we set $\Gamma_c = 10$ dB as a constant, while all other system parameters remain unchanged. The SINR threshold Γ_e is varied from -20dB to 0dB with intervals of 2dB. It should be highlighted that the benchmark curves of [13] remain constant in all the figures of this subsection. This is because these algorithms do not take the PLS into account, hence the change of threshold Γ_e does not affect these performances.

Fig. 7 shows that the radar beampattern MSE decreases upon increasing Γ_e both for the proposed SDR and ZF algorithms. Specifically, we can see that the curves of Fig. 7 remain near-constant, when Γ_e is less than -12dB, while decreasing noticeably, when Γ_e is higher than -10dB. Similar trends may also be observed in Fig. 8 and Fig. 9, which implies that the performance is not sensitive to the choice of Γ_e, when Γ_e is less than -12dB for this set of parameters. Having excessively low Γ_e increases the infeasibility probability of the optimization problem considered.

In Fig. 8, we can see that the system's sum-rate also remains unchanged for the SDR algorithm as a result of the constant threshold Γ_c being close to the optimal solution. By contrast, the curves of ZF show an increasing trend in Fig. 8 upon increasing Γ_e, since a higher Γ_e implies that less severe restrictions are imposed on the ZF-based beamforming.

In Fig. 9, the SDR and the ZF for $K = 4$ reach the boundary of the secrecy rate $\log_2(1+\Gamma_c) - \log_2(1+\Gamma_e)$. Meanwhile, the ZF for $K = 2$ attains a higher secrecy rate than its counterparts, since supporting less LUs imposes less restrictions on the beamforming design. Furthermore, we can infer from Fig. 8 and Fig. 9 that although a low Γ_e reduces the achievable

Authorized licensed use limited to: UNIVERSITY OF SOUTHAMPTON. Downloaded on February 16,2023 at 09:13:26 UTC from IEEE Xplore. Restrictions apply.

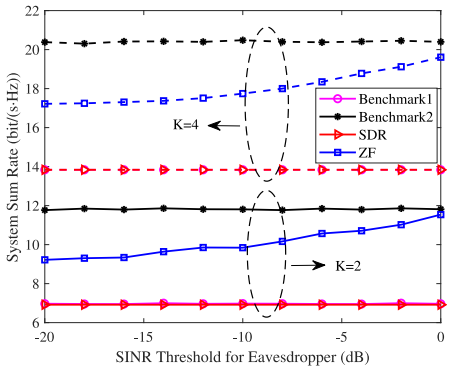

Fig. 8. The achievable sum rate versus SINR threshold Γ_e for Eves, $\Gamma_c = 10$ dB.

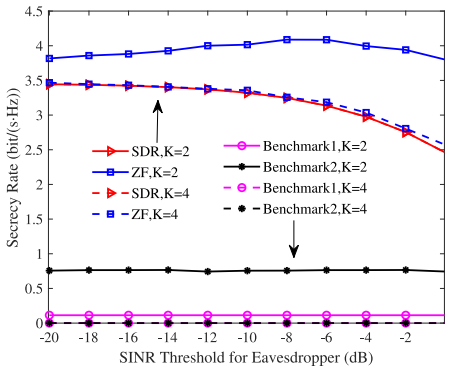

Fig. 9. The secrecy rate versus SINR threshold Γ_e for Eves, $\Gamma_c = 10$ dB.

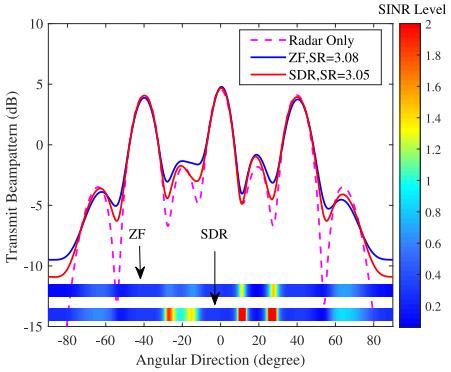

Fig. 10. Transmit beampattern for multiple targets with uncertain directions.

data rate of the Eve, it also results in a low data rate for the LUs. Therefore, no obvious secrecy rate improvement is attained upon reducing Γ_e.

C. System Performance Evaluation for Imperfect CSI

First, we evaluate the impact of angular uncertainties of the Eves on the system performance. We set $Q = 3$ targets having the directions of $\theta_1 = -40°$, $\theta_2 = 0°$, and $\theta_3 = 40°$, respectively. Each target has the same direction uncertainty of $\Delta\theta = 5°$. The BS detects and tracks these targets, while serving $K = 3$ LUs. The SINR thresholds for the LUs and the Eves are set to $\Gamma_c = 10$ dB and $\Gamma_e = 0$ dB, respectively.

Fig. 10 illustrates the radar transmit beampattern synthesized by the proposed algorithms. The SINR level defined

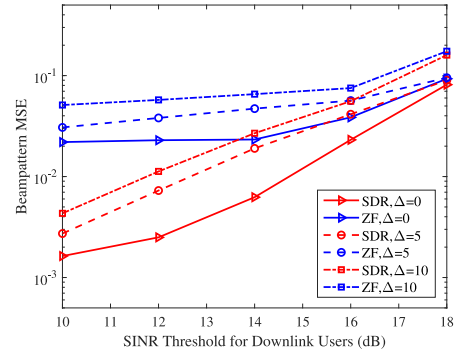

Fig. 11. Beampattern MSE comparison with different angular uncertainties of the Eves.

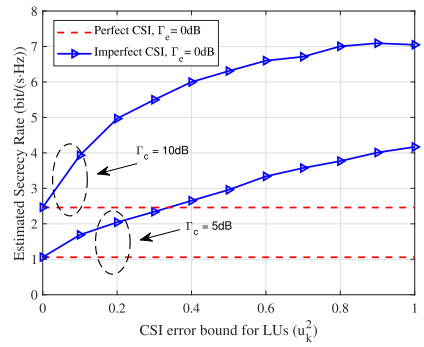

Fig. 12. Estimated secrecy rate calculated by the known imperfect CSI versus error bound.

by (15) is calculated over the set of $[-90°, 90°]$ angular direction. It can be observed that although the BS forms multi-beams pointing to the directions of the Eves, the SINR levels in each interval covering the Eves are controlled by the threshold Γ_e. This is because the signal power of radar waveforms is higher than that of the communication symbols, which have to be protected. Moreover, although the beampattern of the ZF algorithm is less beneficial than that of the SDR (higher side-lobe), the average spatial SINR level is lower than that of the SDR algorithm. In Fig. 11, we evaluate the impact of the direction uncertainties on the optimization performance upon varying Γ_c from 10dB to 18dB. As expected, further constraints are introduced by the uncertainty of the target directions, hence leading to an eroded radar performance.

Fig. 12 shows the estimated secrecy rate calculated by the known imperfect CSI versus the error bound for the scenario of $K = 2$. It can be observed that the estimated secrecy rates remain constant and are equal to the secrecy rates in the case of perfect CSI. By contrast, the curves obtained in the case of imperfect CSI exhibit an increasing trend. This is because the worst-case secrecy rate is forced to be larger than a given threshold in our robust beamforming algorithm, while the statistical difference between the worst-case and estimated secrecy rate becomes larger upon increasing the error bound.

VII. Conclusion

A DFRC multi-user communication system was proposed, while taking the physical layer security into account. The

Authorized licensed use limited to: UNIVERSITY OF SOUTHAMPTON. Downloaded on February 16,2023 at 09:13:26 UTC from IEEE Xplore. Restrictions apply.

weighted sum of the communication signal and radar waveform was adopted for dual-functional transmission. We demonstrated that the additional radar waveform conveying no confidential information improves the DoF in target detection and simultaneously contaminates the eavesdropping channel. Subsequently, the SDR and the low complexity ZF algorithms were proposed for finding the global optimal solution of the formulated non-convex beamforming design problem. Furthermore, we also designed the robust beamforming for the more practical scenarios of imperfect CSI knowledge. Finally, we evaluated the impact of the parameters on the attainable system performance by numerical simulations, which showed an excellent consistency with the theoretical analysis. Designing PLS systems operating in the face of other types of legitimate and eavesdropping channels as well as hardware impairments is left for our future research. Another promising area of research is the design of Pareto-optimal multi-component systems relying on the full set of optimal operating points in terms of throughput, bit error rate (BER), package loss, latency, etc.

Appendix A
The Proof of Proposition 1

By applying the [13, Th. 1], we only have to prove that the PLS constraint (17b) holds for $\tilde{\mathbf{R}}, \tilde{\mathbf{R}}_1, \ldots, \tilde{\mathbf{R}}_K$, if it holds for $\hat{\mathbf{R}}, \hat{\mathbf{R}}_1, \ldots, \hat{\mathbf{R}}_K$. First, we show that

$$\mathbf{a}^H(\theta)\hat{\mathbf{R}}_k\mathbf{a}(\theta) \geq \mathbf{a}^H(\theta)\tilde{\mathbf{R}}_k\mathbf{a}(\theta), \tag{37}$$

for arbitrary θ. Upon substituting the expression of $\tilde{\mathbf{R}}_k$ into (19), the right-hand side term of the inequality can be expanded as

$$\begin{aligned}\mathbf{a}^H\tilde{\mathbf{R}}_k\mathbf{a} &= \mathbf{a}^H\tilde{\mathbf{w}}_k\tilde{\mathbf{w}}_k^H\mathbf{a}\\ &= \left(\mathbf{h}_k^H\hat{\mathbf{R}}_k\mathbf{h}_k\right)^{-1}\mathbf{a}^H\hat{\mathbf{R}}_k\mathbf{h}_k\mathbf{h}_k^H\hat{\mathbf{R}}_k\mathbf{a}\\ &= \left(\mathbf{h}_k^H\hat{\mathbf{R}}_k\mathbf{h}_k\right)^{-1}|\mathbf{a}^H\hat{\mathbf{R}}_k\mathbf{h}_k|^2.\end{aligned} \tag{38}$$

Additionally, according to the Cauchy-Schwarz inequality, we have

$$\left(\mathbf{h}_k^H\hat{\mathbf{R}}_k\mathbf{h}_k\right)\left(\mathbf{a}^H\hat{\mathbf{R}}_k\mathbf{a}\right) \geq |\mathbf{a}^H\hat{\mathbf{R}}_k\mathbf{h}_k|^2. \tag{39}$$

Therefore, it can be readily seen from (38) and (39) that (37) holds. Thus, we can expound as follows

$$\begin{aligned}\mathbf{a}_q^H\tilde{\mathbf{R}}\mathbf{a}_q + \frac{\sigma_e^2}{|\beta|^2} &\overset{(a)}{=} \mathbf{a}_q^H\hat{\mathbf{R}}\mathbf{a}_q + \frac{\sigma_e^2}{|\beta|^2}\\ &\geq \left(1+\Gamma_e^{-1}\right)\mathbf{a}_q^H\sum_{k=1}^{K}\hat{\mathbf{R}}_k\mathbf{a}_q\\ &\overset{(b)}{\geq} \left(1+\Gamma_e^{-1}\right)\mathbf{a}_q^H\sum_{k=1}^{K}\tilde{\mathbf{R}}_k\mathbf{a}_q,\end{aligned} \tag{40}$$

where *(a)* and *(b)* follow the first equation in (19) and the inequality (37), respectively. Thus, the PLS constraint (17b) holds for $\tilde{\mathbf{R}}, \tilde{\mathbf{R}}_1, \ldots, \tilde{\mathbf{R}}_K$, hence completing the proof.

Appendix B
The Proof of Proposition 2

The proof is divided into the following three parts:

(1) We show that the radar covariance matrix $\hat{\mathbf{R}}_{\text{rad}}$ in (29) is a positive semidefinite matrix, hence it can be decomposed by either the Cholesky decomposition or by the square root method. Actually, we have

$$\begin{aligned}&\hat{\mathbf{R}} - \mathbf{W}_c\mathbf{W}_c^H\\ &= \hat{\mathbf{R}} - \hat{\mathbf{R}}_{\text{com}} + \hat{\mathbf{R}}_{\text{com}} - \mathbf{W}_c\mathbf{W}_c^H\\ &= \hat{\mathbf{R}} - \hat{\mathbf{R}}_{\text{com}} + \mathbf{L}_c\left(\mathbf{I} - \left[\mathbf{Q}^H\right]_{[:,1:K]}[\mathbf{Q}]_{[1:K,:]}\right)\mathbf{L}_c^H.\end{aligned} \tag{41}$$

Here, $\hat{\mathbf{R}} - \hat{\mathbf{R}}_{\text{com}}$ is positive semidefinite due to the constraint (26a). Since $[\mathbf{Q}^H]_{[:,1:K]}$ is the sub-matrix containing the first K columns of unitary matrix, $(\mathbf{I} - [\mathbf{Q}^H]_{[:,1:K]}[\mathbf{Q}]_{[1:K,:]})$ is a positive semidefinite matrix, thereby the last term is also positive semidefinite.

(2) We show that the proposed precoding matrices satisfy the ZF constraint (21). Upon letting $\mathbf{F} = \text{diag}(\sqrt{\rho_1}, \ldots, \sqrt{\rho_K})$, we have

$$\mathbf{H}\mathbf{R}_{\text{com}}\mathbf{H}^H = \mathbf{H}\mathbf{L}_c\mathbf{L}_c^H\mathbf{H}^H = \mathbf{L}_h\mathbf{L}_h^H = \mathbf{F}\mathbf{F}^H. \tag{42}$$

Note that $\mathbf{L}_h\mathbf{L}_h^H$ and $\mathbf{F}\mathbf{F}^H$ are the Cholesky decompositions of the matrix $\text{diag}(\boldsymbol{\rho})$, therefore we have $\mathbf{L}_h = \mathbf{F}$ according to the uniqueness of the Cholesky decomposition of a positive definite matrix. Thus, we have

$$\begin{aligned}\mathbf{H}\mathbf{W}_c &= \mathbf{H}\mathbf{L}_c\left[\mathbf{Q}^H\right]_{[:,1:K]}\\ &= \left[\mathbf{L}_h, \mathbf{0}_{K\times(M-K)}\right]\mathbf{Q}\left[\mathbf{Q}^H\right]_{[:,1:K]}\\ &= \mathbf{L}_h = \mathbf{F}.\end{aligned} \tag{43}$$

Moreover, for the radar precoding matrix, we arrive at

$$\begin{aligned}\mathbf{H}\mathbf{W}_r\mathbf{W}_r^H\mathbf{H}^H &= \mathbf{H}\left(\hat{\mathbf{R}} - \mathbf{W}_c\mathbf{W}_c^H\right)\mathbf{H}^H\\ &= \mathbf{F}\mathbf{F}^H - \mathbf{F}\mathbf{F}^H = \mathbf{0}.\end{aligned} \tag{44}$$

Thus we can readily obtain $\mathbf{H}\mathbf{W}_r = \mathbf{0}$ from (44).

(3) We show that the proposed precoding matrices meet the PLS constraint (24). According to the positive semidefinite property, we can show that

$$\mathbf{y}^H\left(\mathbf{I} - \left[\mathbf{Q}^H\right]_{[:,1:K]}[\mathbf{Q}]_{[1:K,:]}\right)\mathbf{y} \geq 0, \tag{45}$$

for an arbitrary non-zero vector $\mathbf{y}$. Upon letting $\mathbf{y} = \mathbf{L}_c^H\mathbf{a}_q$, we have

$$\begin{aligned}&\mathbf{a}_q^H\mathbf{L}_c\left(\mathbf{I} - \left[\mathbf{Q}^H\right]_{[:,1:K]}[\mathbf{Q}]_{[1:K,:]}\right)\mathbf{L}_c^H\mathbf{a}_q\\ &= \mathbf{a}_0^H\hat{\mathbf{R}}_{\text{com}}\mathbf{a}_q - \mathbf{a}_q^H\mathbf{W}_c\mathbf{W}_c^H\mathbf{a}_q \geq 0.\end{aligned} \tag{46}$$

By applying the inequality (46), we can see that

$$\begin{aligned}\mathbf{a}_q^H\hat{\mathbf{R}}\mathbf{a}_q + \frac{\sigma_e^2}{|\beta|^2} &\overset{(a)}{\geq} \left(1+\Gamma_e^{-1}\right)\mathbf{a}_q^H\hat{\mathbf{R}}_{\text{com}}\mathbf{a}_q\\ &\geq \left(1+\Gamma_e^{-1}\right)\mathbf{a}_q^H\mathbf{W}_c\mathbf{W}_c^H\mathbf{a}_q,\end{aligned} \tag{47}$$

Authorized licensed use limited to: UNIVERSITY OF SOUTHAMPTON. Downloaded on February 16,2023 at 09:13:26 UTC from IEEE Xplore. Restrictions apply.

where (a) is valid, because $\hat{\mathbf{R}}$ and $\hat{\mathbf{R}}_{\mathrm{com}}$ are the feasible solution of problem $\mathcal{P}_3$ and $\hat{\mathbf{R}}$ follows the relationship (29). Consequently, it can be observed that the precodering matrix constructs also satisfy the PLS constraint, hence completing the proof.

REFERENCES

[1] F. Liu, C. Masouros, A. P. Petropulu, H. Griffiths, and L. Hanzo, "Joint radar and communication design: Applications, state-of-the-art, and the road ahead," *IEEE Trans. Commun.*, vol. 68, no. 6, pp. 3834–3862, Jun. 2020.

[2] "Number of active IoT devices expected to reach 24.1 billion in 2030." Help Net Security. 2020. [Online]. Available: https://www.helpnetsecurity.com/ 2020/05/22/active-iot-devices

[3] F. Liu et al., "Integrated sensing and communications: Toward dual-functional wireless networks for 6G and beyond," *IEEE J. Sel. Areas Commun.*, vol. 40, no. 6, pp. 1728–1767, Jun. 2022.

[4] Y. Cui, F. Liu, X. Jing, and J. Mu, "Integrating sensing and communications for ubiquitous IoT: Applications, trends, and challenges," *IEEE Netw.*, vol. 35, no. 5, pp. 158–167, Sep./Oct. 2021.

[5] P. Kumari, J. Choi, N. González-Prelcic, and R. W. Heath, "IEEE 802.11ad-based radar: An approach to joint vehicular communication-radar system," *IEEE Trans. Veh. Technol.*, vol. 67, no. 4, pp. 3012–3027, Apr. 2018.

[6] D. Ma, N. Shlezinger, T. Huang, Y. Liu, and Y. C. Eldar, "Joint radar-communication strategies for autonomous vehicles: Combining two key automotive technologies," *IEEE Signal Process. Mag.*, vol. 37, no. 4, pp. 85–97, Jul. 2020.

[7] U. S. Toro, K. Wu, and V. C. M. Leung, "Backscatter wireless communications and sensing in green Internet of Things," *IEEE Trans. Green Commun. Netw.*, vol. 6, no. 1, pp. 37–55, Mar. 2022.

[8] L. Zheng, M. Lops, Y. C. Eldar, and X. Wang, "Radar and communication coexistence: An overview: A review of recent methods," *IEEE Signal Process. Mag.*, vol. 36, no. 5, pp. 85–99, Sep. 2019.

[9] N. C. Luong, X. Lu, D. T. Hoang, D. Niyato, and D. I. Kim, "Radio resource management in joint radar and communication: A comprehensive survey," *IEEE Commun. Surveys Tuts.*, vol. 23, no. 2, pp. 780–814, 2nd Quart., 2021.

[10] F. Liu, C. Masouros, A. Li, H. Sun, and L. Hanzo, "MU-MIMO communications with MIMO radar: From co-existence to joint transmission," *IEEE Trans. Wireless Commun.*, vol. 17, no. 4, pp. 2755–2770, Apr. 2018.

[11] F. Liu, L. Zhou, C. Masouros, A. Li, W. Luo, and A. Petropulu, "Toward dual-functional radar-communication systems: Optimal waveform design," *IEEE Trans. Signal Process.*, vol. 66, no. 16, pp. 4264–4279, Aug. 2018.

[12] S. Shi, Z. Wang, Z. He, and Z. Cheng, "Constrained waveform design for dual-functional MIMO radar-communication system," *Signal Process.*, vol. 171, pp. 1–11, Jun. 2020.

[13] X. Liu, T. Huang, N. Shlezinger, Y. Liu, J. Zhou, and Y. C. Eldar, "Joint transmit beamforming for multiuser MIMO communications and MIMO radar," *IEEE Trans. Signal Process.*, vol. 68, pp. 3929–3944, Jun. 2020.

[14] X. Li et al., "Physical layer security of cognitive ambient backscatter communications for green Internet-of-Things," *IEEE Trans. Green Commun. Netw.*, vol. 5, no. 3, pp. 1066–1076, Sep. 2021.

[15] N. Su, F. Liu, Z. Wei, Y.-F. Liu, and C. Masouros, "Secure dual-functional radar-communication transmission: Exploiting interference for resilience against target eavesdropping," *IEEE Trans. Wireless Commun.*, vol. 21, no. 9, pp. 7238–7252, Sep. 2022.

[16] K. Wu, J. A. Zhang, X. Huang, and Y. J. Guo, "Integrating secure communications into frequency hopping MIMO radar with improved data rate," *IEEE Trans. Wireless Commun.*, vol. 21, no. 7, pp. 5392–5405, Jul. 2022.

[17] A. Deligiannis, A. Daniyan, S. Lambotharan, and J. A. Chambers, "Secrecy rate optimizations for MIMO communication radar," *IEEE Trans. Aerosp. Electron. Syst.*, vol. 54, no. 5, pp. 2481–2492, Oct. 2018.

[18] B. K. Chalise and M. G. Amin, "Performance tradeoff in a unified system of communications and passive radar: A secrecy capacity approach," *Digit. Signal Process.*, vol. 82, pp. 282–293, Nov. 2018.

[19] N. Su, F. Liu, and C. Masouros, "Secure radar-communication systems with malicious targets: Integrating radar, communications and jamming functionalities," *IEEE Trans. Wireless Commun.*, vol. 20, no. 1, pp. 83–95, Jan. 2021.

[20] S. Goel and R. Negi, "Guaranteeing secrecy using artificial noise," *IEEE Trans. Wireless Commun.*, vol. 7, no. 6, pp. 2180–2189, Jun. 2008.

[21] R. W. Heath, N. González-Prelcic, S. Rangan, W. Roh, and A. M. Sayeed, "An overview of signal processing techniques for millimeter wave MIMO systems," *IEEE J. Sel. Topics Signal Process.*, vol. 10, no. 3, pp. 485–500, Apr. 2016.

[22] E. Tuncer and B. Friedlander, *Classical and Modern Direction-of-Arrival Estimation*. New York, NY, USA: Academic, 2009.

[23] Z. Yang, J. Li, P. Stoica, and L. Xie, "Sparse methods for direction-of-arrival estimation," in *Academic Press Library in Signal Processing*, vol. 7, R. Chellappa and S. Theodoridis, Eds. London, U.K.: Academic, 2018, pp. 509–581.

[24] C. Sturm and W. Wiesbeck, "Waveform design and signal processing aspects for fusion of wireless communications and radar sensing," *Proc. IEEE*, vol. 99, no. 7, pp. 1236–1259, Jul. 2011.

[25] Z.-M. Jiang et al., "Intelligent reflecting surface aided dual-function radar and communication system," *IEEE Syst. J.*, vol. 16, no. 1, pp. 475–486, Mar. 2022.

[26] P. Stoica, J. Li, and Y. Xie, "On probing signal design for MIMO radar," *IEEE Trans. Signal Process.*, vol. 55, no. 8, pp. 4151–4161, Aug. 2007.

[27] Y.-F. Liu, Y.-H. Dai, and Z.-Q. Luo, "Coordinated beamforming for MISO interference channel: Complexity analysis and efficient algorithm," *IEEE Trans. Signal Process.*, vol. 59, no. 3, pp. 1142–1157, Mar. 2011.

[28] A. Mukherjee and A. L. Swindlehurst, "Robust beamforming for security in MIMO wiretap channels with imperfect CSI," *IEEE Trans. Signal Process.*, vol. 59, no. 1, pp. 351–361, Jan. 2011.

[29] R. H. Tütüncü, K. C. Toh, and M. J. Todd, "Solving semidefinite-quadratic-linear programs using SDPT3," *Math. Program.*, vol. 95, no. 2, pp. 189–217, 2003.

[30] M. Grant and S. Boyd, "CVX: MATLAB software for disciplined convex programming, version 2.2." 2020. [Online]. Available: http://cvxr.com/cvx

[31] Z.-Q. Luo, W.-K. Ma, A. M.-C. So, Y. Ye, and S. Zhang, "Semidefinite relaxation of quadratic optimization problems," *IEEE Signal Process. Mag.*, vol. 27, no. 3, pp. 20–34, May 2010.

[32] P. Stoica, J. Li, and X. Zhu, "Waveform synthesis for diversity-based transmit beampattern design," *IEEE Trans. Signal Process.*, vol. 56, no. 6, pp. 2593–2598, Jun. 2008.

[33] X. Zhang, *Matrix Analysis and Applications*. Cambridge, U.K.: Cambridge Univ. Press, 2017.

[34] Q. H. Spencer, A. L. Swindlehurst, and M. Haardt, "Zero-forcing methods for downlink spatial multiplexing in multiuser MIMO channels," *IEEE Trans. Signal Process.*, vol. 52, no. 2, pp. 461–471, Feb. 2004.

[35] A. Wiesel, Y. C. Eldar, and S. Shamai, "Zero-forcing precoding and generalized inverses," *IEEE Trans. Signal Process.*, vol. 56, no. 9, pp. 4409–4418, Sep. 2008.

[36] F. Liu, C. Masouros, T. Ratnarajah, and A. Petropulu, "On range sidelobe reduction for dual-functional radar-communication waveforms," *IEEE Wireless Commun. Lett.*, vol. 9, no. 9, pp. 1572–1576, Sep. 2020.

[37] F. Wang, X. Wang, and Y. Zhu, "Transmit beamforming for multiuser downlink with per-antenna power constraints," in *Proc. IEEE Int. Conf. Commun. (ICC)*, Jun. 2014, pp. 4692–4697.

[38] K.-C. Toh, "An inexact primal–dual path following algorithm for convex quadratic SDP," *Math. Program.*, vol. 112, no. 1, pp. 221–254, Mar. 2008.

Authorized licensed use limited to: UNIVERSITY OF SOUTHAMPTON. Downloaded on February 16,2023 at 09:13:26 UTC from IEEE Xplore. Restrictions apply.